JOURNAL OF MATERIALS SCIENCE 28 (1993) 4704–4712

Effects of changes in strain path on the anisotropy of yield stresses of low-carbon steel and 70–30 brass sheets

JAE HWAN CHUNG, DONG NYUNG LEE
Department of Metallurgical Engineering and Center for Advanced Materials Research, Seoul National University, Seoul 151-742, Korea

Uniaxial tensile tests in various directions following uniaxial extension, equibiaxial stretching or plane strain rolling have been performed to study the effects of changes in strain path on the anisotropy of yield stresses of aluminium-killed low-carbon steel and 70–30 brass sheets. The anisotropy could be predicted from the specimen textures, if dislocation structure were equiaxed, as in the case of equibiaxial stretching. However, elongated dislocation cell structures, developed in the steel specimens prestrained in uniaxial tension or plane strain rolling, gave rise to the second-stage yield stresses higher than predicted from textures in the directions different from the maximum prestrain direction. Planar dislocation structures in the brass specimens prestrained in uniaxial tension or plane strain rolling gave the second-stage yield stresses lower than predicted from the textures in the directions different from the maximum prestrain direction. The phenomena are discussed based on textures and dislocation structures.

1. Introduction

In sheet-forming processes, sheet metals are formed to final products through sequential forming processes. It has been found that changes in strain path during plastic deformation of the metals give rise to flow stresses and strain-hardening rates which differ from those expected from monotonic deformation. Changes in strain hardening, residual ductility and homogeneity of strain paths are important factors for accurate modelling of stamping processes. Ghosh and Backofen [1] classified the behaviour of materials which were subjected to uniaxial tension after biaxial prestraining into ferritic and non-ferritic types. The ferritic type (as in aluminium-killed steel) shows increases in yield stresses and decreases in strain-hardening rates in the second-stage extensions. On the other hand, the non-ferritic type (as in 70–30 brass) shows premature yielding and an increase in the strain-hardening rate. The transient deformation behaviour tends to increase with increasing strain in prestraining. The uniaxial tension followed by uniaxial tension in directions different from the prestrain direction yields, in general, a higher yield stress, lower strain-hardening rate and premature strain instability in the ferritic-type materials (AK steel) and a lower yield stress and higher strain-hardening rate in the non-ferritic-type materials (70–30 brass) [2–5]. The second-stage yield stresses and strain-hardening rates are known to be transient and finally approach those in prestraining [6, 7]. Factors affecting the mechanical properties due to the strain path changes may be the shape and size of grains, second-phase particles, crystallographic texture, dislocation structure and others. For commercial aluminium-killed low-carbon steel and 70–30 brass sheets, the effects of the shape and size of the grain and second-phase particles on the anisotropy of yield stresses are expected to be not very important. The effect of textures on the anisotropy of yield stresses can be evaluated reasonably well [8, 9]. Therefore, the relative importance of the dislocation structure may be estimated.

The objective of this study was to investigate effects of the texture and dislocation structure on the mechanical properties due to path changes of uniaxial–uniaxial extension, equibiaxial stretching–uniaxial extension and plane strain–uniaxial extension of the AK low-carbon steel and 70–30 brass sheets.

2. Experimental procedure

2.1. Measurements of mechanical properties

Temper-rolled aluminium-killed low-carbon steel sheet (0.8 mm thick and 14 μm grain size) and 70–30 brass sheet (0.7 mm, 20 μm) specimens whose chemical compositions are given in Table I were subjected to tensile tests at 0°, 22.5°, 45°, 67.5° and 90° to the rolling direction at a crosshead speed of 5 mm min^{-1}. The strain-rate sensitivities were measured by changing the crosshead speed from 5 mm min^{-1} to 50 mm min^{-1} at 15% strain. The plastic strain ratios (the ratio of plastic width strain to thickness strain) were also measured at 15% strain. The measured tensile properties of the steel and brass specimens are given in Table II. Three types of strain path changes were carried out. They are three types of prestraining (uniaxial extension, equibiaxial stretching and plane

0022–2461

TABLE I Chemical compositions of materials in the steel and the brass (%)

Steel								Brass				
C	Si	Mn	P	S	Ni	Cr	Al	Cu	Al	Fe	Pb	Zn
0.062	0.035	0.210	0.011	0.011	0.015	0.040	0.040	69.8	0.003	0.011	0.012	30.1

TABLE II Tensile properties of as-received steel and brass sheet specimens (25 mm gauge length)

	Angle (deg)	YS (MPa)	UTS (MPa)	Uniform elong. (%)	Total elong. (%)	n^a	$n(n')^a$	m^b	R
Steel	0	153.9	287.3	28.8	50.4	0.250		0.0141	1.964
	22.5	157.1	191.9	28.2	50.0	0.245		0.0138	1.837
	45	163.4	294.7	28.2	49.6	0.241		0.0142	1.491
	67.5	158.5	289.6	28.4	50.8	0.243		0.0140	2.052
	90	152.0	282.9	29.0	52.0	0.250		0.0143	2.661
	$\bar{X}$	158.0	290.3	28.4	50.4	0.245		0.0141	1.924
Brass	0	118.5	335.7	57.2	65.2		0.550(0.478)		0.939
	22.5	117.3	331.9	56.0	66.4		0.545(0.480)		1.047
	45	116.1	329.1	58.8	70.8		0.560(0.488)		1.057
	67.5	119.4	331.3	57.6	67.2		0.533(0.475)		1.027
	90	118.9	333.6	59.2	71.6		0.563(0.491)		1.024
	$\bar{X}^a$	117.9	332.7	57.7	68.7		0.554(0.482)		1.028

[a] n and n' are hardening exponents obtained from all the data and those around strain 0.4, respectively.
[b] Strain-rate sensitivity.
[c] Strain ratio.
[d] $\bar{X} = \frac{1}{8}(X_0 + 2X_{22.5} + 2X_{45} + 2X_{67.5} + X_{90})$.

strain rolling) followed by uniaxial extension, and will be referred to as uniaxial–uniaxial extension, equibiaxial stretching–uniaxial extension and plane strain–uniaxial extension. The dimension of specimens for prestraining in uniaxial tension is shown in Fig. 1. The specimens were tensile strained in the rolling direction by 5%, 10%, 15%, 20% and 25%, from which the second-stage tensile specimens were cut at 0°, 22.5°, 67.5° and 90° to the prestrain direction. Equibiaxial stretching of sheets was obtained using the equipment shown in Fig. 2. From the stretched sheet, tensile specimens were cut at 0° 22.5°, 45°, 67.5° and 90° to the rolling direction. The plane strain deformation was achieved by rolling by 5%, 10% and 15% in the rolling direction. In order to obtain homogeneous deformation during rolling, sufficient lubrication and small reduction per pass were applied. From the rolled sheets, the tensile specimens used in the second-stage deformation were machined at 0°, 22.5°, 45°, 67.5° and 90° to the rolling direction. The second-stage tensile specimens were subjected to tensile tests.

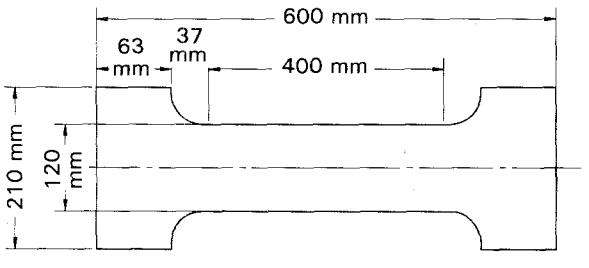

Figure 1 Dimensions of the tensile specimen for prestraining in uniaxial tension.

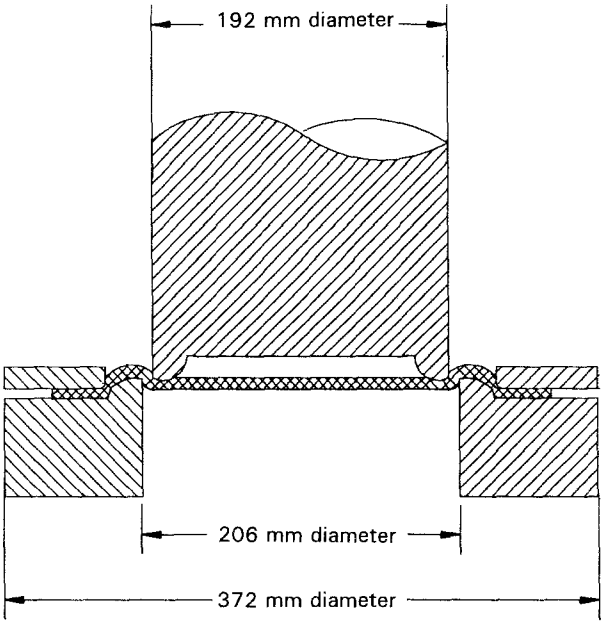

Figure 2 Punch and die set for equibiaxial stretching.

2.2. Measurements of texture and TEM structures

The (1 1 0), (2 0 0) and (2 1 1) pole figures for the AK steel sheets and the (1 1 1), (2 0 0) and (2 2 0) pole figures for 70–30 brass sheets were measured. The pole figure data were used to calculate the orientation distribution functions. The TEM structures of specimens were observed under 200 kV Jeol TEM.

3. Results

3.1. Mechanical properties

3.1.1. Uniaxial–uniaxial extension

Fig. 3 shows uniaxial flow curves of the AK low-carbon steel specimens tested at 45° and 90° to the prestrain direction after prestraining in uniaxial tension in the rolling direction (RD). Relative to the flow strengths attained at equivalent strains in monotonic deformation, the changes in strain path were accompained by substantial increases in the initial flow stress. The increase was more prominent in the 45° test, as shown in Fig. 4. Tensile behaviour of the 70–30 brass was different from that of the AK steel, as shown in Fig. 5. The strain path change following a small

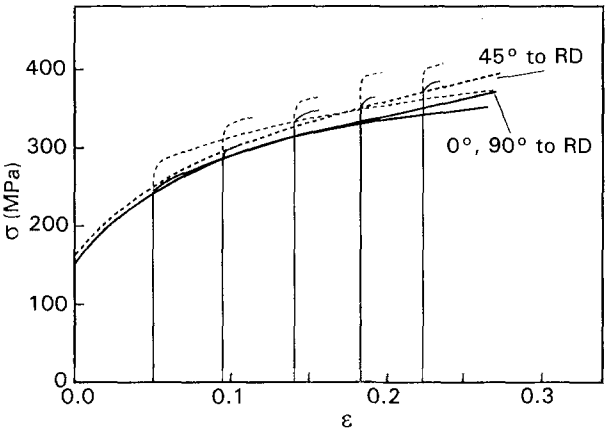

Figure 3 Flow curves of the AK steel specimens tested at (– – –) 45° and (——) 90° to the prestrain direction after prestraining in uniaxial tension in the rolling direction (RD).

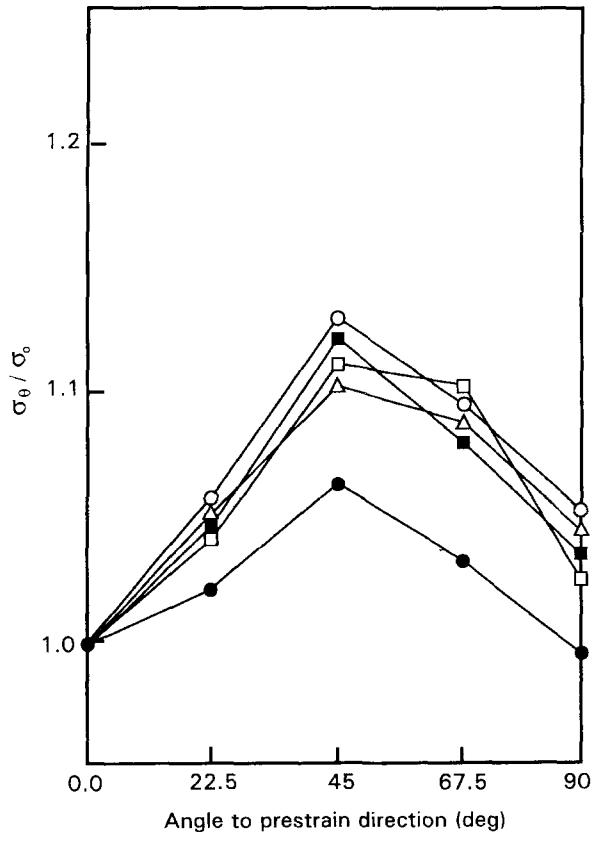

Figure 4 Anisotropy of the second-stage yield stresses of the AK steel specimens tested after prestraining in uniaxial tension in the RD. Prestrain: (●) 0, (■) 0.049, (□) 0.095, (△) 0.140, (○) 0.182.

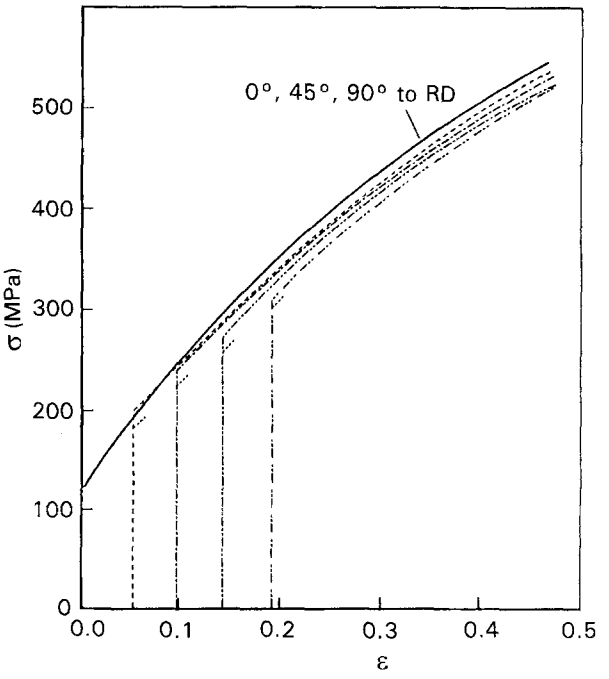

Figure 5 Flow curves of the 70–30 brass specimens tested at 45° and (· · · ·) 90° to the prestrain direction after prestraining in uniaxial tension in the RD. The 90° curves are shortened to avoid complication, but they are almost parallel to the 45° curves. Prestrain at 45°: (– – –) 0.049, (— · —) 0.095, (— · · —) 0.140, (— · · — · ·) 0.182.

prestraining in uniaxial tension in the RD caused an increase in the 45° second-stage yield stress. However, the second-stage yield stresses decreased with increasing prestrain with higher values at 45° to the RD (Fig. 6).

3.1.2. Equibiaxial stretching–uniaxial extension

Plastic behaviour of the AK steel specimens tested in the RD after prestraining in equibiaxial tension is shown in Fig. 7. In order for comparison with monotonic flow behaviour, it is necessary to introduce an appropriate effective strain. The Hosford yield equation [10] for anisotropic materials yields the following effective strain [11]

$$\bar{\varepsilon} = (1 + R)^{1/a}[1 + |\alpha|^a + R|1 - \alpha|^a]^{(a-1)/a} \left[1 + R\frac{|1 - \alpha|^a}{(1 - \alpha)}\right]^{-1} \varepsilon_1 \quad (1)$$

where R is the plastic strain ratio (the ratio of width to thickness strain), α is the ratio of transverse stress to longitudinal stress (σ_2/σ_1), a is a constant (6 for bcc, 8 for fcc) and ε_1 is the longitudinal strain ($\alpha = 1$). For equibiaxial streching, the effective strain reduces to

$$\bar{\varepsilon} = 2^{(a-1)/a}(1 + R)^{1/a}\varepsilon_1 \quad (2)$$

The effective strains give rise to higher yield stresses than expected from the monotonic flow curve. The Hosford yield criterion was obtained based on Taylor's minimum energy [12] for yielding of crystalline materials. The equibiaxial stretching also reduced variation in the second-stage yield stress with tensile

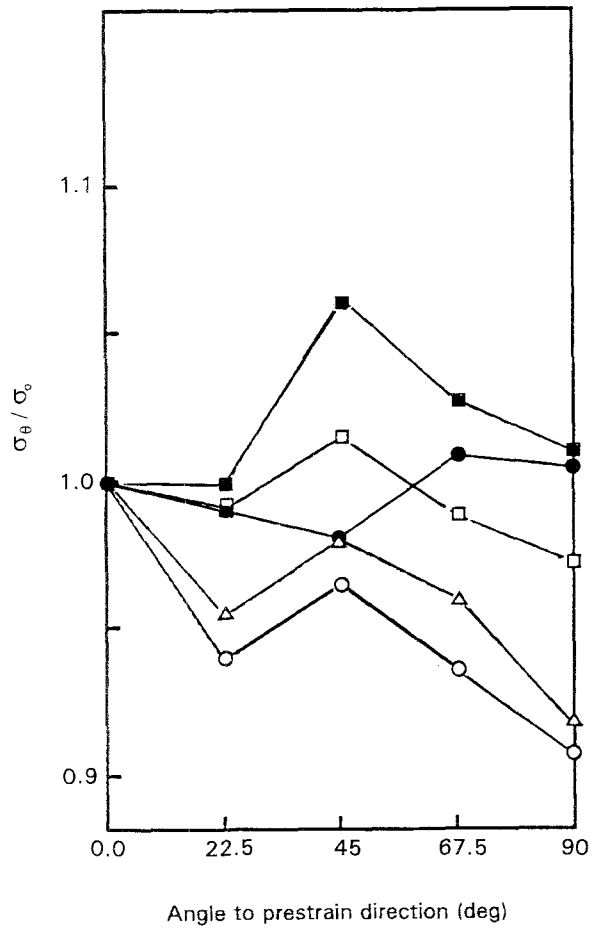

Figure 6 Anisotropy of the second-stage yield stresses of the 70–30 brass specimens after prestraining in uniaxial tension in the RD. Prestrain: (●) 0, (■) 0.049, (□) 0.095, (△) 0.140, (○) 0.182.

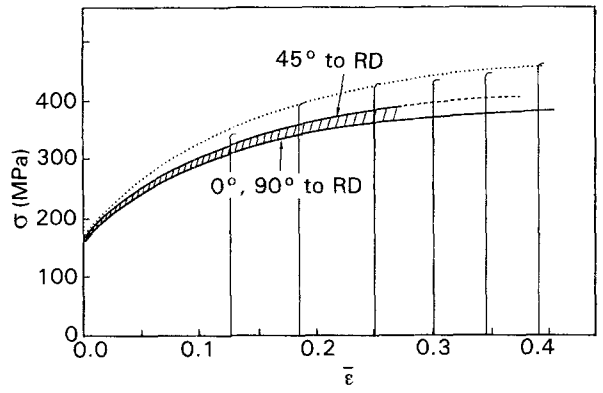

Figure 7 Plastic behaviour of the AK steel tested at the RD after prestraining in equibiaxial tension. The effective strain, $\bar{\varepsilon}$, was calculated based on the Hosford yield criterion.

direction as shown in Fig. 8. Fig. 9 shows the second-stage flow curves of 70–30 brass specimens tested in the RD after prestraining in equibiaxial tension. The effective strain was calculated using Equation 2. The agreement between the monotonic and second-stage flow curves indicates that the effective strain defined in Equation 1 is satisfactory in the brass specimens.

3.1.3. Plane strain–uniaxial extension

Fig. 10 shows the second-stage flow curves of AK steel specimens tensile tested after plane strain rolling in which the maximum principal strain direction was

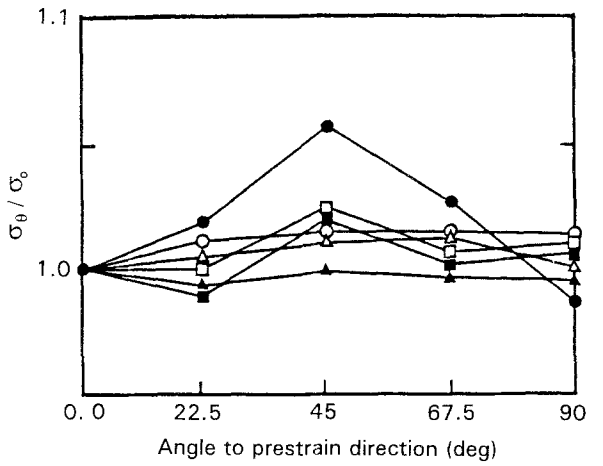

Figure 8 Anisotropy of the second-stage yield stresses of the AK steel specimens tested after prestraining in equibiaxial tension. Effective prestrain: (●) 0, (■) 0.125, (□) 0.184, (△) 0.252, (○) 0.345, (▲) 0.434.

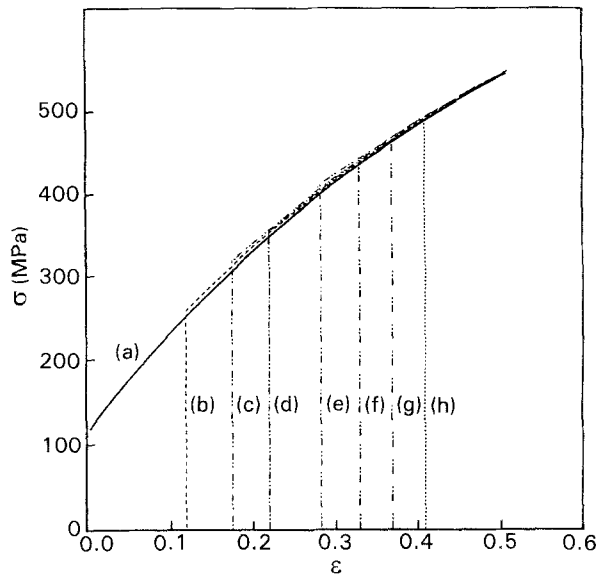

Figure 9 The second-stage flow curves of the 70–30 brass tested in the RD after prestraining in equibiaxial tension. The effective strains were calculated based on the Hosford yield criterion: (a) 0, (b) 0.117, (c) 0.172, (d) 0.218, (e) 0.280, (f) 0.323, (g) 0.365, (h) 0.406.

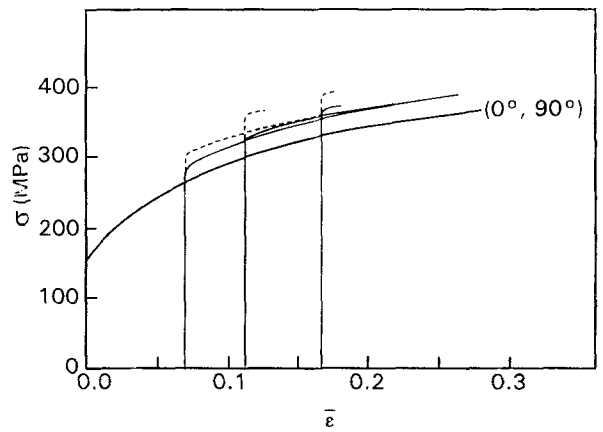

Figure 10 The second-stage flow curves of the AK steel tested after plane strain prestraining in which the maximum principal strain direction is parallel to RD. The effective strain was calculated based on the Hosford yield criterion. (– – –) 0° to maximum prestrain direction, (——) 90° to maximum prestrain direction.

parallel to the rolling direction. The effective strain in prestraining was calculated based on Equation 1. For plane strain

$$\rho = \frac{d\varepsilon_2}{d\varepsilon_1} = \frac{|\alpha|^a(1-\alpha) - R|1-\alpha|^a\alpha}{\alpha(1-\alpha+R|1-\alpha|^a)} = 0 \quad (3)$$

Substitution of Equation 3 into Equation 1 gives

$$\bar{\varepsilon} = (1+R)^{1/a}\left\{1 + \left[\frac{R^{1/(a-1)}}{1+R^{1/(a-1)}}\right]^{(a-1)}\right\}^{-1/a}\varepsilon_1 \quad (4)$$

The yield stresses obtained in the second-stage flow curves are higher than expected from the monotonic extensions. On the other hand, the second-stage flow curves of 70–30 brass are not very different from that expected from the monotonic extensions, but indicate slightly higher flow stresses at low prestrains and lower flow stresses at higher prestraining (Fig. 11).

3.2. Crystallographic textures

Fig. 12a shows the (1 1 0) pole figure and ODF for the AK steel sheet in the as-received state. The sheet had

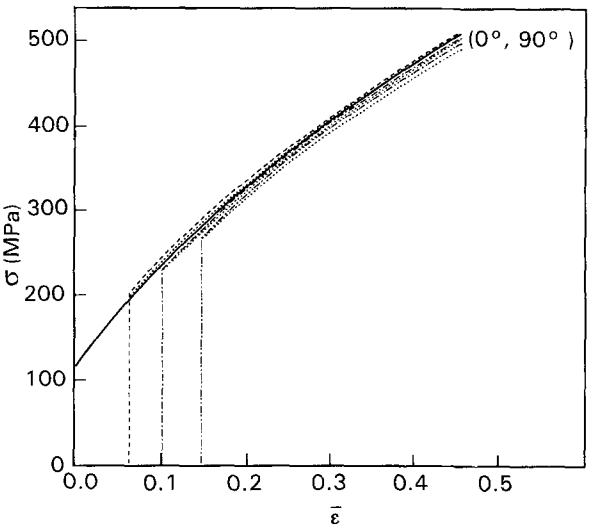

Figure 11 The second-stage flow curves of the 70–30 brass tested after plane strain prestraining. Effective prestrain; (——) 0, (– – –) 0.063 (0°), (— · —) 0.104 (0°), (— · · —) 0.152 (0°), (· · ·) 90°. "0°" indicates that the maximum principal strain direction in prestraining is parallel to the RD. The effective strains were calculated based on the Hosford yield criterion.

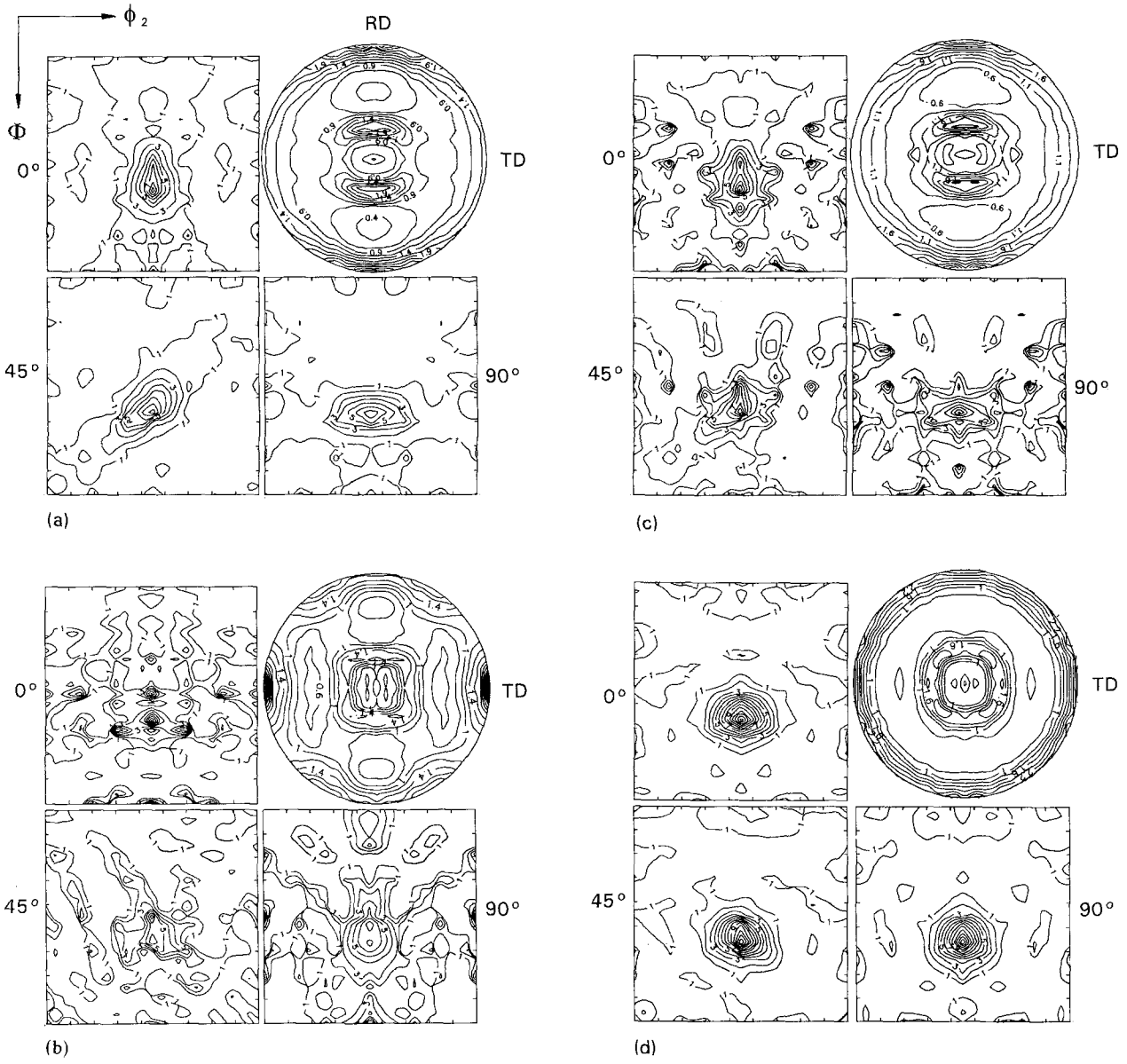

Figure 12 (1 1 0) pole figures and ODFs for the AK steel sheets (a) in the as-received state, (b) prestrained by 0.182 in uniaxial tension at the RD, (c) plane strain rolled by an effective strain = 0.167, and (d) prestrained in equibiaxial tension by an effective strain = 0.299. The numbers on the left and right of ODFs indicate ϕ_1 values.

a relatively well-developed (1 1 1) fibre texture. When prestrained in uniaxial tension in the RD and rolled by effective strain of 0.167, the fibre texture was disturbed as shown in Fig. 12b and c. However, the specimen stretched in equibiaxial tension showed a very well-developed (1 1 1) fibre texture as shown in Fig. 12d. Fig. 13a shows the (1 1 1) pole figure and ODF for the 70–30 brass sheet in the as-received state, which indicate a poorly developed texture. Prestraining by 0.182 in uniaxial tension and by rolling by an effective strain of 0.152 developed slightly stronger textures in the sheets as shown in Fig. 13b and c. Equibiaxial stretching gave rise to a weak fibre texture as shown in Fig. 13d.

3.3. TEM structures

Fig. 14 shows well-developed dislocation cell structures in the AK steel specimens, whereas rather homogeneous structures were obtained in the brass specimens (Fig. 15). The difference in dislocation structures of the steel and brass specimens is known to be due to a difference in stacking fault energies of the two different materials. The high stacking fault energy tends to develop the cell structure, whereas the low stacking fault energy develops planar and homogeneous dislocation structure. It is also noted that, for steel specimens, elongated cell structures were developed by uniaxial tension and rolling, whereas equibiaxial stretching gave rise to an equiaxed cell structure.

4. Discussion

The anisotropy of yield stresses can be caused by texture. The effect of texture on the yield stress can be calculated based on Taylor's minimum energy theory [8, 9, 12]. Fig. 16 shows the measured second-stage yield stresses of low-carbon steel and 70–30 brass specimens as a function of angle to the rolling direction after equibiaxial stretching as compared with

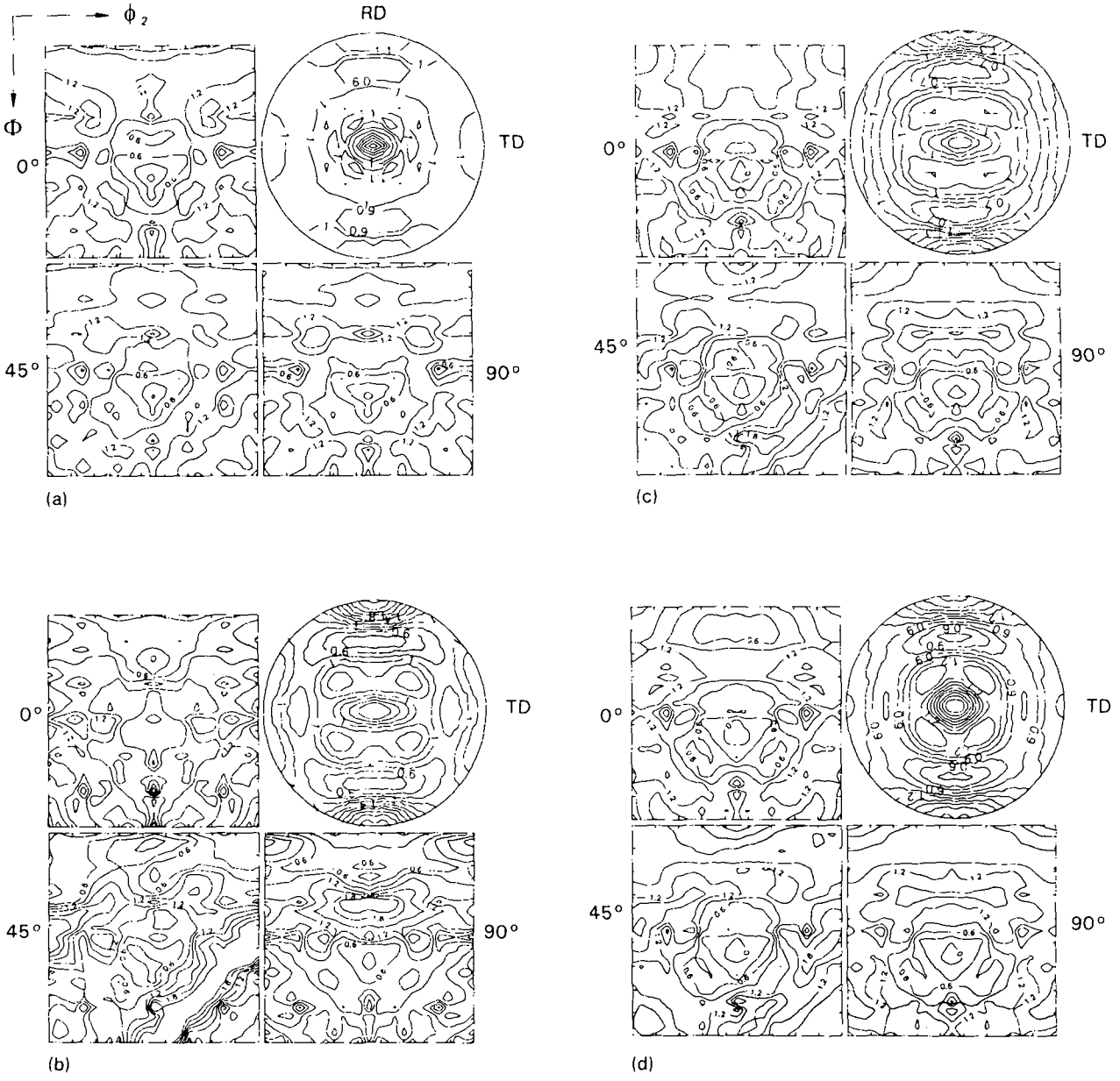

Figure 13 (1 1 1) pole figures and ODFs for the 70–30 brass sheets (a) in the as-received state, (b) prestrained by 0.182 in uniaxial tension at the RD, (c) plane strain rolled by effective strain 0.152, and (d) prestrained in equibiaxial tension by effective strain 0.280. The numbers on the left and right of ODFs indicate ϕ_1 values.

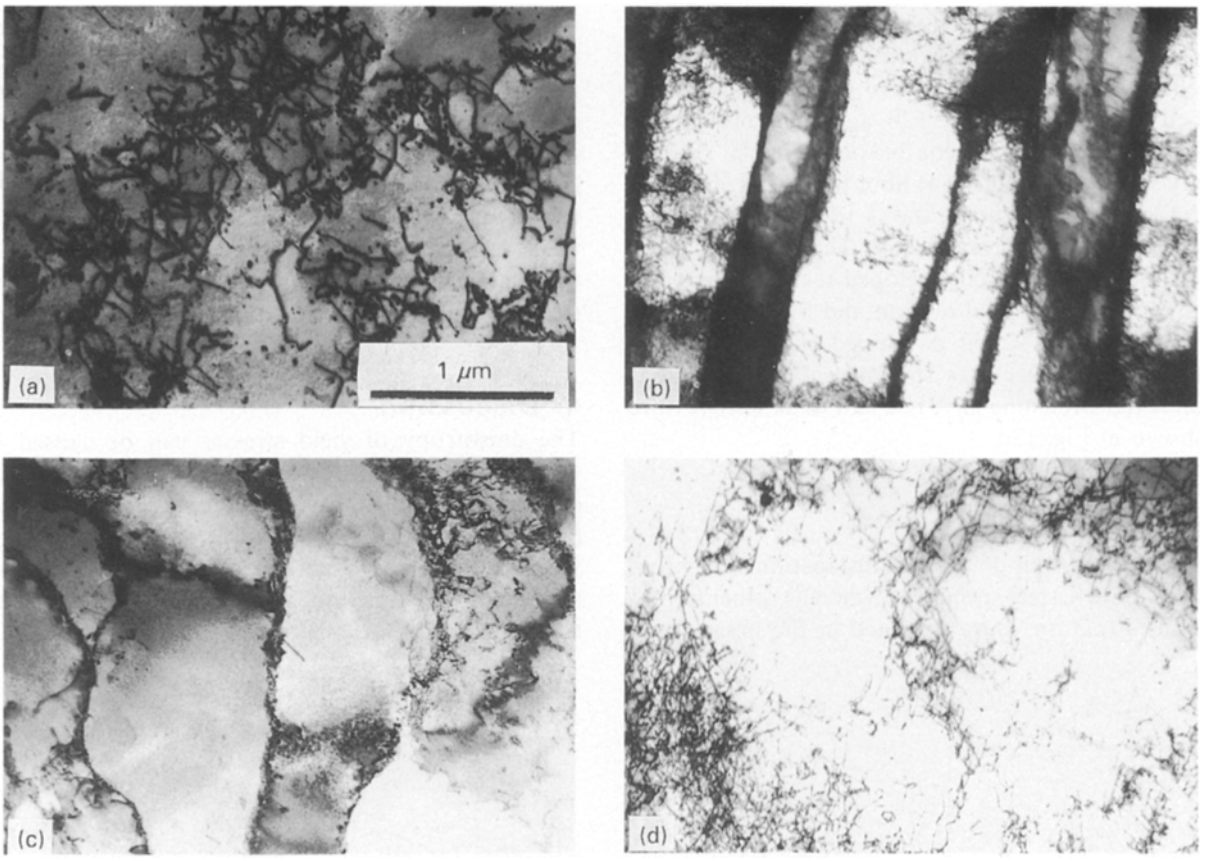

Figure 14 TEM structures of the AK steel specimens (a) in the as-received state, (b) after prestraining in uniaxial tension ($\varepsilon = 0.182$), (c) after prestraining by rolling ($\bar{\varepsilon} = 0.167$), and (d) after prestraining in equibiaxial tension ($\bar{\varepsilon} = 0.126$).

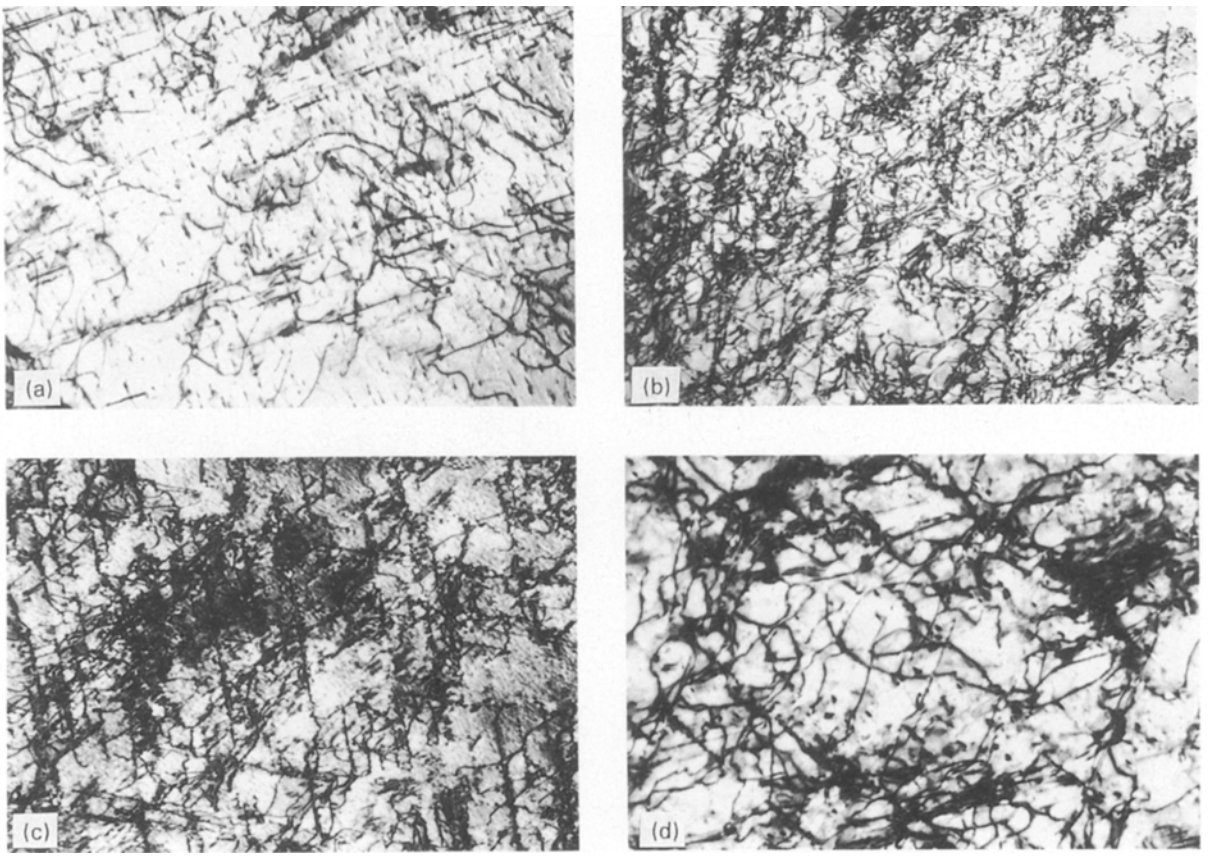

Figure 15 TEM structures of the 70–30 brass specimens (a) in the as-received state, (b) after prestraining in uniaxial tension ($\varepsilon = 0.182$), (c) after prestraining by rolling ($\bar{\varepsilon} = 0.152$) and (d) after prestraining in equibiaxial tension ($\bar{\varepsilon} = 0.28$).

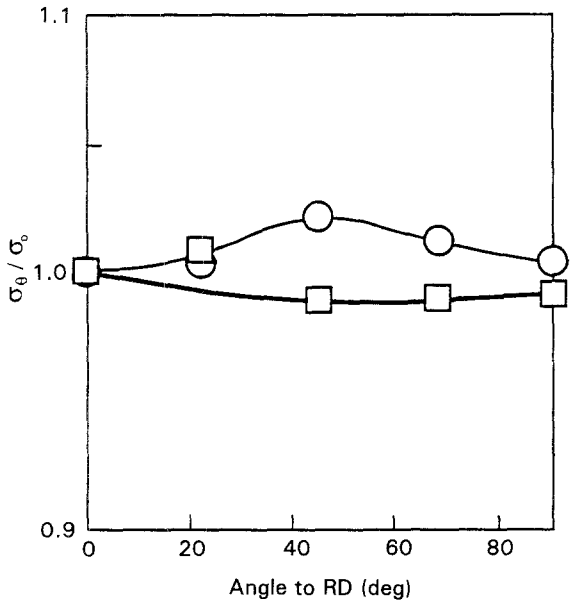

Figure 16 The second-stage yield stresses of (○) the AK steel and (□) the 70–30 brass specimens tested after prestraining in equibiaxial tension ($\bar{\varepsilon} = 0.299$ for steel and $\bar{\varepsilon} = 0.28$ for brass). The curves indicate values calculated based on textures.

those calculated based on textures. The equibiaxial stretching made the dislocation structure more equiaxed as shown in Figs 14d and 15d. Therefore, the anisotropy of yield stresses in Fig. 16 is expected to be caused mainly by the textures of specimens. The excellent agreement between measured data and values calculated using textures reflects that the calculation gives us satisfactory texture effects.

Fig. 17 show anisotropy of yield stresses of the as-received AK steel and 70–30 brass specimens as a function of angle to the rolling direction. For brass, the measured data are in good agreement with values calculated based on textures due to isotropic dislocation structure as shown in Fig. 15a. On the other hand, the steel specimens show a little disagreement between measured and calculated values, possibly due to a slight anisotropic dislocation structure developed during temper rolling, even though it cannot be clearly seen in Fig. 14a.

When tested in different strain paths after prestraining in uniaxial tension in the rolling direction, the yield stress of low-carbon steel specimens deviated positively from the values calculated from their textures, whereas those of 70–30 brass specimens deviated negatively from the calculated values, as shown in Fig. 18. This behaviour can be attributed to the differences in dislocation structures of the two different alloys. The steel specimens had elongated dislocation cell structures as shown in Fig. 14b. If a strain path change takes place, the relatively stable elongated cell walls developed during prestraining will become barriers to dislocation movement due to the new extension. Therefore the second-stage yield stress after the strain path change must be higher than that in the uniaxial prestraining. In this case, a 90° change in strain path will give rise to the highest increase. This may be the case of steel specimens in Fig. 19, because uniaxial tension and rolling of steel specimens caused elongated cell structure as shown in Fig. 14c. However, for the steel specimen in Fig. 18, the highest increase was observed in a 45° change in strain path, even though they had elongated cell structures (Fig. 14b). The same phenomenon was found in brass specimens.

Brass specimens prestrained in uniaxial tension behave very differently from steel specimens as shown in Fig. 18. As mentioned earlier, dislocation structures in brass specimens are planar and relatively homogeneous due to their low stacking fault energy. Therefore,

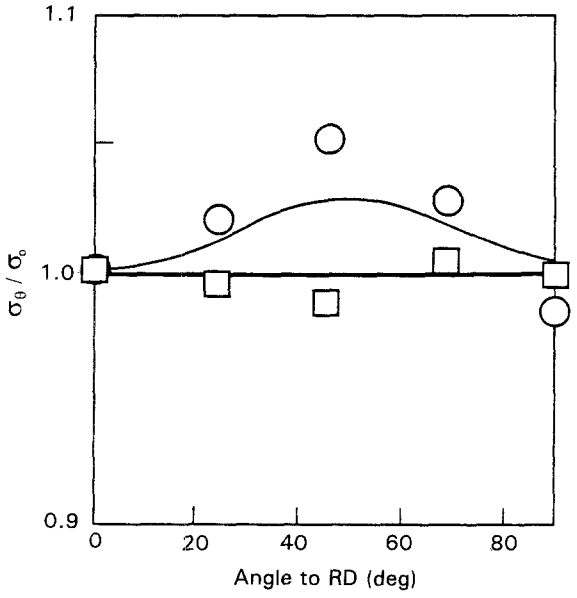

Figure 17 The yield stresses of (○) the AK steel and (□) 70–30 brass specimens in the as-received state. The upper and lower curves are values calculated using textures of steel and brass specimens, respectively.

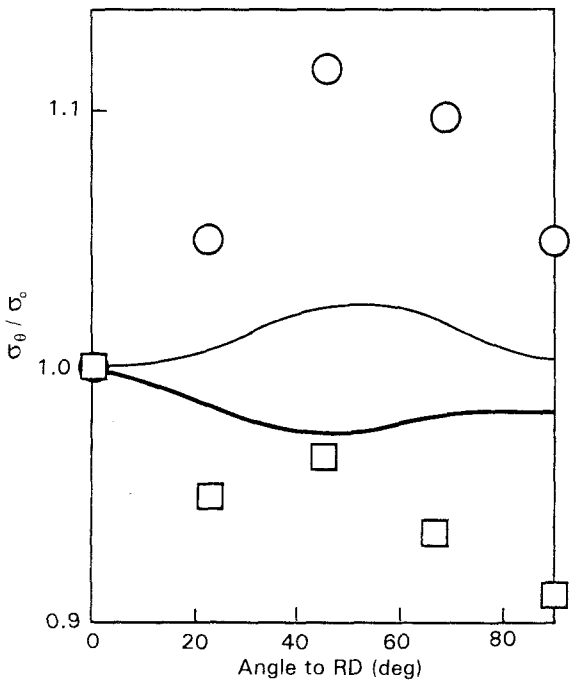

Figure 18 The second-stage yield stresses of (○) the AK steel and (□) 70–30 brass specimens tested after prestraining in uniaxial tension ($\varepsilon = 0.182$). The upper and lower curves are values calculated using textures of steel and brass specimens, respectively.

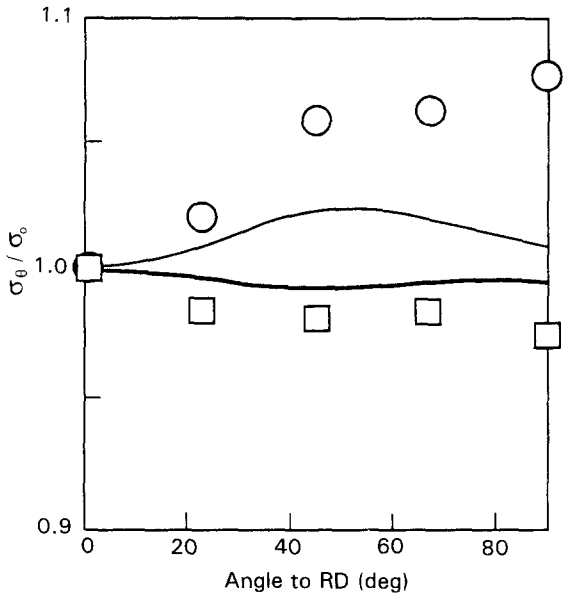

Figure 19 The yield stesses of (○) the AK steel and (□) 70–30 brass specimens after prestraining by rolling ($\bar{\varepsilon} = 0.167$ for steel and $\bar{\varepsilon} = 0.152$ for brass) The upper and lower curves are values calculated using textures of steel and brass specimens, respectively.

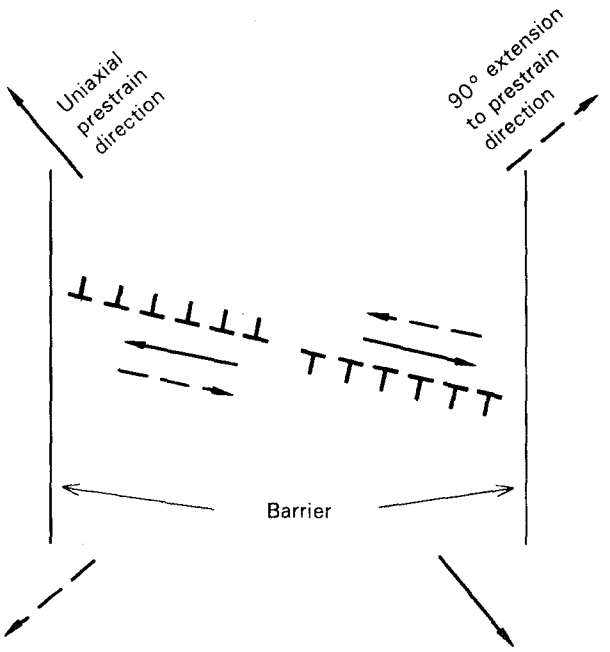

Figure 20 Schematic drawing explaining dislocations generated by uniaxial extension being moved towards the opposite direction by 90° extension to the prior uniaxial extension.

the anisotropic yielding behaviour of brass in Fig. 18 cannot be explained as in low-carbon steel. The planar dislocation structure may be approximated by dislocation pile ups as shown in Fig. 20. The figure indicates that uniaxial extension in the rolling direction followed by uniaxial tension in the transverse direction is similar to uniaxial extension followed by uniaxial compression in the rolling direction which causes the Bauschinger effect, unless slip systems in the both cases are different. Therefore, the second-stage yield stress of the brass specimen tested after a 90° change in strain path is lower than that expected from its texture. However, when tested after a 45° change in strain path, the dislocations generated during prestraining are in the most difficult position of movement, which in turn gives rise to the higher yield stress as shown in Fig. 18. The decrease in the second-stage yield stresses with increasing prestrain is attributed to increasing back stress due to increasing dislocation density with increasing plastic deformation (Fig. 6). This explanation could be applied to the low-carbon steel specimens which show the 45° yield stress higher than that expected. The second-stage yield stresses of brass specimens prestrained by rolling (Fig. 19) deviate less from those calculated using textures than specimens prestrained in uniaxal tension. This may be due to the fact that the number of active slip systems in plane strain deformation (as in rolling) is larger than that in uniaxial tension.

Acknowledgements

This work was financially supported by Korea Science and Engineering Foundation. The Authors also thank Mr Jaewook Kwon, Seoul National University, for his help with experiments and helpful discussion.

References

1. A. K. GHOSH and W. A. BACKOFEN, Metall. Trans. **4** (1973) 1113.
2. D. J. LLOYD and H. SANG, *ibid.* **10a** (1979) 1767.
3. W. B. HUTCHINSON, R. ARTHERY and P. MALMSTROM, *Scripta Metall.* **10** (1976) 673.
4. A. J. RANTA-ESKOLA, *Met. Technol.* **8** (1980) 45.
5. J. V. LAUKONIS, *Metall. Trans.* **12A** (1981) 467.
6. J. L. PAPHANEL, J. H. SCHMITT and B. BAUDELET, *Int. J. Plast.* **2** (1986) 371.
7. M. ZANDRAHIMI, S. PLATIAS, D. PRICE, D. BARRETT, P. S. BATE, W. T. ROBERTS and D. V. WILSON, *Metall. Trans.* **20A** (1989) 2471.
8. H. J. BUNGE, "Texture Analysis in Materials Science" (Butterworths, London, 1982) p. 330.
9. D. N. LEE, K. H. OH and I. S. KIM, *J. Mater. Sci.* **23** (1988) 4013.
10. W. F. HOSFORD, in "Proceedings of the 7th North American Metal Working Conference", SME, Dearbon MI (1979) p. 191.
11. D. N. LEE and Y. K. KIM, in "Forming Limit Diagrams; Concepts, Methods and Applications", edited by R. H. Wagoner, K. S. Chan and S. P. Keeler, (TMS-AIME, Warrendale, PA, 1989) p. 153.
12. G. I. TAYLOR, *J. Inst. Met.* **62** (1938) 307.

Received 27 April 1992
and accepted 24 February 1993